Underactuated Leader-Follower Synchronisation for Multi-Agent Systems with Rejection of Unknown Disturbances

D.J.W. Belleter and K.Y. Pettersen

***Abstract*— In this paper leader-follower synchronization is considered for underactuated followers in an inhomogeneous multi-agent system. The goal is to synchronise the motion of a leader and an underactuated follower. Measurements of the leader's position and velocity are available, while the dynamics and trajectory of the leader is unknown. The leader velocities are used as input for a constant bearing guidance algorithm to assure that the follower synchronises its motion to the leader. It is also shown that the proposed leader-follower scheme can be applied to multi-agent systems that are subjected to unknown environmental disturbances. Furthermore, the trajectory of the leader does not need to be known. The stability properties of the complete control scheme and the unactuated internal dynamics are analysed using nonlinear cascaded system theory. Simulation results are presented to validate the proposed control strategy.**

I. Introduction

This paper considers leader-follower output feedback synchronization for inhomogeneous multi-agent systems with underactuated agents. Leader-follower synchronization has several applications concerning both autonomous and nonautonomous vehicles. Leader-follower synchronization can for instance be applied to underway replenishment operations, robot manipulator master-slave synchronisation, and formation control tasks.

Leader-follower synchronization for underway replenishment has been investigated in for instance [1] and [2]. In [1] the case of a fully actuated follower that synchronizes its output with a leader with unknown dynamics is investigated. The velocities of the leader and the follower are assumed to be unknown and have to be estimated using an observer. The observer-controller scheme utilized in [1] is based on theory for master-slave synchronization of robotic manipulators investigated in [3]. In [2] the interaction forces between two vessels are investigated during underway replenishment. A constant bearing guidance algorithm from [4] is used to synchronize the ships along a straight line path. The vessels are underactuated, but no environmental disturbances are considered. In [5] underway replenishment between fully actuated vessels is investigated and adaptive backstepping controllers are designed to reject exogenous disturbances.

Leader-follower synchronization is also widely applied in coordinated control. Applications include master-slave synchronization of robot manipulators in [3], leader-follower synchronization of mobile robots in [6]–[9], and formation control of marine vessels in [10]. For these applications the models are either fully actuated or formulated only at the kinematic level. However, most commercial systems are underactuated or become underactuated at higher speed, i.e. vessels with a tunnel thruster to apply a sideways force is fully actuated for low speeds but the tunnel thruster becomes inefficient at cruising speed, see [11] and the references therein. Furthermore, cars and most mobile robots are also underactuated (non-holonomic) systems. A formation control strategy that can be applied to underactuated multi-agent systems is considered in [12] where hybrid control techniques are used. The approach is based on consensus rather than leader-follower synchronisation and does not take into account disturbance rejection. In [13] formation control of underactuated vessels under the influence of constant disturbances is considered using neural network adaptive dynamic surface control to track pre-defined paths.

In [14] formation control of underactuated systems is considered, and straight-line path following in formation is achieved for underactuated marine vessels under the influence of constant ocean currents. Straight-line target tracking for underactuated unmanned surface vessels is investigated in [15]. In [15] constant bearing guidance is used to track a target moving in a straight line, experimental results are presented but closed loop stability is not proven.

The case considered in this paper is leader-follower synchronisation for an underactuated follower in an inhomogeneous multi-agent system. The multi-agent system can thus consist of a leader with arbitrary dynamics as long as it moves in the same space as the follower(s). The follower can be any type of vehicle described by the nonlinear manoeuvring model that is introduced in the next section. For formation control purposes each follower can again be the leader of other followers, or all followers can have the same leader. Examples of possible configurations are autonomous surface vessels (ASV) following an autonomous underwater vehicle (AUV) as communication nodes during AUV search and survey operations, or a fleet of ASVs manoeuvring by following a leader. Since we consider an underactuated system we need to take into account the full dynamic model in the control design and analysis. In particular, since the system is underactuated it is not possible to consider a purely kinematic model, and also it is not possible for the case considered here to perform feedback linearisation of the full dynamics. In addition to taking into account the follower's underactuation, we also take into account that the follower is

This work was partly supported by the Research Council of Norway through its Centres of Excellence funding scheme, project No. 223254 AMOS.

D.J.W. Belleter and K.Y. Pettersen are with the Centre for Autonomous Marine Operations and Systems (AMOS) and the Department of Engineering Cybernetics, Norwegian University of Science and Technology, NO7491 Trondheim, Norway {dennis.belleter,kristin.y.pettersen}@itk.ntnu.no.

affected by unknown environmental disturbances. The leader dynamics and the leader trajectories are assumed to be unknown. The leader is free to move as it wants independently of the follower, but the follower has access to measurements of the leader's position and velocity in the inertial frame. This includes cases where there is communication between the leader and follower, but also when the follower reads AIS measurements of the leader [16].

It should be noted that the leader-follower synchronisation scheme in this paper has its dual problem in trajectory tracking. Hence, the input signal of the leader could easily be replaced by a virtual leader. This is true for most, if not all, leader-follower type synchronisation schemes since the leader can always be represented as a virtual vehicle with known trajectory and properties. When, however, the strategy is applied in a chained form, i.e. followers become leaders to other vehicles, this duality is lost. The stability properties derived in this work will still hold with respect to each leader. However, in future work string stability should be investigated to analyse the error propagation along the chain of vehicles.

The class of systems and disturbances considered in this paper is the same as in [14]. However, the formation control strategy in [14] is trajectory dependent. More specifically, it is designed for straight-line path following in formation and the path following task is (partially) decoupled from the formation task, and the path planning is made a priori, while in this paper the path is chosen online by the leader during the mission, and these tasks are coupled in order to achieve synchronisation to the leader. Furthermore, in [14] it is assumed that each vessel is disturbed by the same current. This limitation does not apply to this work. Moreover, whereas [14] allows for mutual synchronisation with leader-follower behaviour as a special case, this work is strictly aimed at leader-follower behaviour.

The paper is organised as follows. In Section II the dynamic model for the follower and the constant bearing guidance algorithm are introduced. The closed-loop behaviour is investigated in Section III. Section IV presents simulations considering different scenarios. Finally Section V gives the conclusions of the work.

II. The Follower

This section presents the model for the follower and the guidance law for the follower that is used to synchronise its motion to that of the leader. The leader-follower synchronisation scheme is developed for a class of systems described by a 3-DOF manoeuvring model. This class of systems includes underactuated autonomous surface vessels (ASV) and autonomous underwater vehicles (AUV) moving in the horizontal plane. However, it should be noted that the developed leader-follower scheme can be extended to different classes of systems by considering the appropriate dynamic model, control/guidance scheme, and appropriate disturbances.

A. The Vessel Model

We consider an ASV or AUV moving in the horizontal plane. The motion of the vessel is described by the position and orientation of the vessel w.r.t. the earth-fixed reference frame, i.e. $\eta \triangleq [x, y, \psi]^T$. For marine craft the earth-fixed north-east-down (NED) frame is usually used as inertial frame [17]. The vector of linear and angular velocities is given in the body-fixed reference frame by $\nu \triangleq [u, v, r]^T$, containing the surge velocity u, sway velocity v, and yaw rate r. The vessel is disturbed by an ocean current expressed in the inertial frame n, i.e. the earth-fixed frame. The current is denoted by $\boldsymbol{V_c}$ and satisfies the following assumption.

Assumption 1: The ocean current is assumed to be constant and irrotational w.r.t. n, i.e. $\boldsymbol{V_c} \triangleq [V_x, V_y, 0]^T$. Furthermore, it is bounded by $V_{\max} > 0$ such that $\|V_c\| = \sqrt{V_x^2 + V_y^2} \leq V_{\max}$.

The ocean current velocity expressed in the body-fixed frame b is denoted by $\nu_c \triangleq [u_c, v_c, 0]^T$. It can be obtained by $\nu_c = \boldsymbol{R}(\psi)^T \boldsymbol{V}_c$ where $\boldsymbol{R}(\psi)$ is the rotation matrix from the body to inertial frame defined as

$$\boldsymbol{R}(\psi) \triangleq \begin{bmatrix} \cos(\psi) & -\sin(\psi) & 0 \\ \sin(\psi) & \cos(\psi) & 0 \\ 0 & 0 & 1 \end{bmatrix}. \tag{1}$$

The vessel model is expressed in terms of the relative velocity defined as $\nu_r \triangleq \nu - \nu_c = [u_r, v_r, r]^T$ expressed in b. Since the ocean current is constant and irrotational the vessel can be described by the 3-DOF manoeuvring model [17]

$$\dot{\eta} = \boldsymbol{R}(\psi)\nu_r + \boldsymbol{V}_c \tag{2a}$$

$$\boldsymbol{M}\dot{\nu}_r + \boldsymbol{C}(\nu_r)\nu_r + \boldsymbol{D}\nu_r = \boldsymbol{B}\boldsymbol{f} \tag{2b}$$

The vector $\boldsymbol{f} \triangleq [T_u, T_r]^T$ is the control input vector, containing the surge thrust T_u and the rudder angle T_r. The matrix $\boldsymbol{M} = \boldsymbol{M}^T > 0$ is the system inertia matrix including added mass, $\boldsymbol{C}$ is the Coriolis and centripetal matrix, $\boldsymbol{D} > 0$ is the hydrodynamic damping matrix, and $\boldsymbol{B}$ is the actuator configuration matrix.

Remark 1: By expressing the model in relative velocities the environmental disturbances can be incorporated in the model more easily and controlled more straightforwardly.

Assumption 2: We assume port-starboard symmetry.

Remark 2: Assumption 2 is to the authors' best knowledge satisfied for all commercial surface and underwater vessels.

The matrices $\boldsymbol{M}$, $\boldsymbol{D}$, and $\boldsymbol{B}$ are constant and are defined as

$$\boldsymbol{M} \triangleq \begin{bmatrix} m_{11} & 0 & 0 \\ 0 & m_{22} & m_{23} \\ 0 & m_{23} & m_{33} \end{bmatrix}, \boldsymbol{D} \triangleq \begin{bmatrix} d_{11} & 0 & 0 \\ 0 & d_{22} & d_{23} \\ 0 & d_{23} & d_{33} \end{bmatrix}, \boldsymbol{B} \triangleq \begin{bmatrix} b_{11} & 0 \\ 0 & b_{22} \\ 0 & b_{32} \end{bmatrix}.$$

The non-constant matrix $\boldsymbol{C}(\nu_r)$ can be derived from $\boldsymbol{M}$ (See [17]).

Assumption 3: It is assumed the position of the body-fixed frame is chosen such that $\boldsymbol{M}^{-1}\boldsymbol{B}\boldsymbol{f} = [\tau_u, 0, \tau_r]^T$.

Remark 3: This is possible as long as the center of mass is located along the centreline of the vessel. Coordinate transformations for this translation can be found in [18].

Moreover, the position of the body-fixed frame is chosen such that $\boldsymbol{M}^{-1}\boldsymbol{B}\boldsymbol{f} = [\tau_u, 0, \tau_r]^T$.

The model can be written in component form as

$$\dot{x} = u_r \cos(\psi) - v_r \sin(\psi) + V_x \tag{3a}$$
$$\dot{y} = u_r \sin(\psi) + v_r \cos(\psi) + V_y \tag{3b}$$
$$\dot{\psi} = r, \tag{3c}$$
$$\dot{u}_r = F_{u_r}(v_r, r) + \tau_u, \tag{3d}$$
$$\dot{v}_r = X(u_r)r + Y(u_r)v_r, \tag{3e}$$
$$\dot{r} = F_r(u_r, v_r, r) + \tau_r, \tag{3f}$$

which is clearly underactuated in sway. Therefore tracking has to be achieved by a suitable velocity and heading assignment. For this purpose constant bearing guidance is used. The definitions of F_{u_r}, $X(u_r)$, $Y(u_r)$, and F_r are given in Appendix I. Note that $X(u_r)$ and $Y(u_r)$ are bounded for bounded arguments and $Y(u_r)$ satisfies the following assumption.

Assumption 4: It is assumed that $Y(u_r)$ satisfies

$$Y(u_r) \leq -Y_{\min} < 0, \, \forall u_r \in [-V_{\max}, U_{\max}].$$

with $U_{\max}$ the maximal surge speed of the follower.

Remark 4: This assumption is satisfied for commercial vessels by design, since $Y(u_r) \geq 0$ would imply an undamped or nominally unstable vessel is sway direction.

B. Constant Bearing Guidance

This subsection briefly describes constant bearing guidance (CB) as presented in [17] and [4]. CB guidance assigns a desired velocity based on two different components. The first component is the velocity of the leader $\boldsymbol{v}_l^n = [\dot{x}_m, \dot{y}_m]^T$ which needs to be matched. The second component is the follower-leader approach velocity $\boldsymbol{v}_a^n$ which is proportional to the relative position in the earth-fixed frame between the follower and the leader $\tilde{\boldsymbol{p}}^n = [\tilde{x}^n, \tilde{y}^n]^T$ and is aligned along the line-of-sight (LOS) vector. The superscript n denotes that the variable is expressed in the earth-fixed frame. An illustration of the constant bearing guidance can be seen in Figure 1. The desired velocity assignment for constant bearing guidance is given by

$$\boldsymbol{v}_d^n = \boldsymbol{v}_l^n + \boldsymbol{v}_a^n \tag{4}$$
$$\boldsymbol{v}_a^n = -\kappa \frac{\tilde{\boldsymbol{p}}^n}{\|\tilde{\boldsymbol{p}}^n\|} \tag{5}$$

with $\boldsymbol{v}_l^n$ the leader velocity, $\boldsymbol{v}_a^n$ the approach velocity, and

$$\tilde{\boldsymbol{p}}^n \triangleq \boldsymbol{p}^n - \boldsymbol{p}_l^n \tag{6}$$

is the LOS vector between the follower and the leader, where $\|\tilde{\boldsymbol{p}}^n\| \geq 0$ is the euclidean length of this vector and

$$\kappa = U_{a,\max} \frac{\|\tilde{\boldsymbol{p}}^n\|}{\sqrt{(\tilde{\boldsymbol{p}}^n)^T \tilde{\boldsymbol{p}}^n + \Delta_{\tilde{p}}^2}} \tag{7}$$

with $U_{a,\max}$ the maximum approach speed and $\Delta_{\tilde{p}}$ a tuning parameter to affect the transient leader-follower rendezvous behaviour.

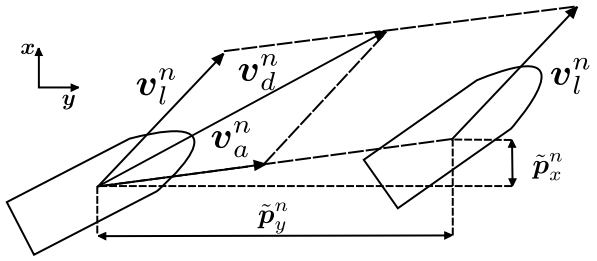

Fig. 1. Constant bearing guidance velocity assignments and position error.

Remark 5: Note that in order to converge to a point that is at a desired off-set w.r.t the leader $\boldsymbol{p}_r$, the position of the leader should be included in (6) as $\boldsymbol{p}_l^n \triangleq \boldsymbol{p}_{l,\text{true}}^n + \boldsymbol{R}(\psi_l)\boldsymbol{p}_r$ where $\boldsymbol{R}(\psi_l)$ is a rotation matrix describing the orientation of the leader. For curved paths the velocity $\boldsymbol{v}_l^n$ should then also be calculated in the off-set point to track the curvature with minimal error.

As shown in [17] the stability and convergence of the CB guidance scheme can be investigated using the positive definite, radially unbounded Lyanpunov function candidate (LFC)

$$V = \frac{1}{2}(\tilde{\boldsymbol{p}}^n)^T \tilde{\boldsymbol{p}}^n \tag{8}$$

Time differentiation of (8) along the trajectories of $\tilde{\boldsymbol{p}}^n$ gives

$$\begin{aligned} \dot{V} &= (\tilde{\boldsymbol{p}}^n)^T(\boldsymbol{v}_d^n - \boldsymbol{v}_l^n) = -\kappa \frac{(\tilde{\boldsymbol{p}}^n)^T \tilde{\boldsymbol{p}}^n}{\|\tilde{\boldsymbol{p}}^n\|} \\ &= -U_{a,\max} \frac{(\tilde{\boldsymbol{p}}^n)^T \tilde{\boldsymbol{p}}^n}{\sqrt{(\tilde{\boldsymbol{p}}^n)^T \tilde{\boldsymbol{p}}^n + \Delta_{\tilde{p}}^2}} < 0, \quad \forall \, \tilde{\boldsymbol{p}}^n \neq 0 \end{aligned} \tag{9}$$

with $\boldsymbol{v}_d^n - \boldsymbol{v}_l^n = \boldsymbol{v}_a^n$ by definition. Hence, the origin $\tilde{\boldsymbol{p}}^n = 0$ is uniformly globally asymptotically stable (UGAS).

The desired heading ψ_d is calculated by extracting heading information from the inner- and outerproducts of the desired velocity $\boldsymbol{v}_d^n$ and the actual velocity $\boldsymbol{v}^n$ [15]. This assures that $\boldsymbol{v}^n$ is aligned with $\boldsymbol{v}_d^n$. More details about constant bearing guidance can be found in [17] and the references therein.

C. The Controller

The control goals are

$$\lim_{t\to\infty} \tilde{\boldsymbol{p}}^n = \boldsymbol{0} \tag{10}$$
$$\lim_{t\to\infty} \tilde{\boldsymbol{v}}^n \triangleq \boldsymbol{v}^n - \boldsymbol{v}_d^n = 0 \tag{11}$$
$$\lim_{t\to\infty} \tilde{\psi} \triangleq \psi - \psi_d = 0 \tag{12}$$

which corresponds to synchronisation with the leader, i.e. that the follower vessel follows the leader, with a constant desired relative position, and with the desired velocity and heading. In this section, we present feedback linearising controllers using the desired velocity and heading angle from II-B, in order to achieve these control goals.

Since the follower is underactuated we can only control the velocity in (3d). Therefore we transform the velocity error

in the earth-fixed frame to an error in the body-fixed frame using the coordinate transformation:

$$\begin{bmatrix}\tilde{\psi}\\ \tilde{u}_r\\ \tilde{v}_r\end{bmatrix} = \begin{bmatrix}1 & 0 & 0\\ 0 & \cos(\tilde{\psi}+\psi_d) & \sin(\tilde{\psi}+\psi_d)\\ 0 & -\sin(\tilde{\psi}+\psi_d) & \cos(\tilde{\psi}+\psi_d)\end{bmatrix}\begin{bmatrix}\tilde{\psi}\\ \tilde{\boldsymbol{v}}^n\end{bmatrix}. \quad (13)$$

It is straightforward to show that the Jacobian of this transformation is given by:

$$\frac{\partial T}{\partial(\tilde{\psi},\tilde{\boldsymbol{v}}^n)} = \begin{bmatrix}1 & 0 & 0\\ -\tilde{v}_x^n\mathrm{s}(\cdot)+\tilde{v}_y^n\mathrm{c}(\cdot) & \mathrm{c}(\cdot) & \mathrm{s}(\cdot)\\ -\tilde{v}_x^n\mathrm{c}(\cdot)-\tilde{v}_y^n\mathrm{s}(\cdot) & -\mathrm{s}(\cdot) & \mathrm{c}(\cdot)\end{bmatrix} \quad (14)$$

with $\mathrm{s}(\cdot) = \sin(\tilde{\psi}+\psi_d)$ and $\mathrm{c}(\cdot) = \cos(\tilde{\psi}+\psi_d)$. The Jacobian (14) can easily be verified to be non-singular. Consequently, T is a global diffeomorphism. A physical interpretation of this is that when $\tilde{\psi}$ is driven to zero, i.e. $\boldsymbol{v}^n$ is aligned with $\boldsymbol{v}_d^n$ by the CB guidance algorithm, the relative surge velocity error can be used to control $\boldsymbol{v}^n$ to $\boldsymbol{v}_d^n$.

Remark 6: For the underactuated model considered here only $\tilde{u}_r = u_r - u_d$ can be used for control purposes, while for the fully actuated case $\tilde{v}_r = v_r - v_d$ could be used to control the sway velocity. For the underactuated case the heading controller assures that $\boldsymbol{v}^n$ is aligned with $\boldsymbol{v}_d^n$ and the control action can be prescribed solely by the surge actuator.

Remark 7: Note that this coupling between the heading and velocity control is what allows for the disturbance rejection. Since if a larger velocity (or smaller) velocity is needed to compensate the effect of the current, the heading controller will assure the vessel is rotated such that $\boldsymbol{v}^n$ and $\boldsymbol{v}_d^n$ are aligned and hence the vessel keeps the correct course.

We will use the following feedback linearising P controller for the surge velocity:

$$\tau_u = -F_{u_r}(v_r, r) + \dot{u}_d - k_{u_r}(u_r - u_d), \quad (15)$$

with $k_{u_r} > 0$ a constant controller gain. To control the yaw rate we use the following controller:

$$\tau_r = -F_r(u_r, v_r, r) + \ddot{\psi}_d - k_\psi(\psi - \psi_d) - k_r(\dot{\psi} - \dot{\psi}_d), \quad (16)$$

with $k_\psi > 0$ and $k_r > 0$ constant controller gains. We introduce the vector $\boldsymbol{\xi} \triangleq [\tilde{u}_r, \tilde{\psi}, \tilde{r}]^T$, with the tracking errors $\tilde{u}_r \triangleq u_r - u_d$, $\tilde{\psi} \triangleq \psi - \psi_d$, and $\tilde{r} \triangleq r - \dot{\psi}_d$. The dynamics of $\boldsymbol{\xi}$ can be found by applying the controllers (15) and (16) to the dynamical system (3) resulting in:

$$\dot{\boldsymbol{\xi}} = \begin{bmatrix}-k_{u_r} & 0 & 0\\ 0 & 0 & 1\\ 0 & -k_\psi & -k_r\end{bmatrix}\boldsymbol{\xi} \triangleq \Sigma\boldsymbol{\xi}. \quad (17)$$

The system (17) is linear and time-invariant and k_{u_r}, k_ψ, and k_r are strictly positive. Consequently, Σ is Hurwitz and the origin of (17) is uniformly globally exponentially stable (UGES) and hence the controllers guarantee exponential tracking of the desired references.

III. Closed Loop Analysis

In this section the stability of the closed-loop system is considered. First, we consider the external dynamics, consisting of the position error dynamics ($\tilde{\boldsymbol{p}}^n = [\tilde{x}, \tilde{y}]^T$), the controlled states (surge velocity, yaw, and yaw rate), and prove that this is UGAS. Secondly, the internal dynamics, i.e. the sway dynamics, are analysed and shown to be practically stable, and the region of stability is seen to be a function of the desired yaw rate.

The analysis of the convergence properties of the CB algorithm from [17], which was presented in Subsection II-B of this paper, assumes that $\boldsymbol{v}^n = \boldsymbol{v}_d^n$ i.e. that the state that is used as a virtual control input has converged to the desired value. In this section we analyse the closed loop system with the CB guidance algorithm and the controller presented in Subsection II-C. Considering the closed loop implies that the constant bearing guidance algorithm of Subsection II-B is considered with $\boldsymbol{v}_d^n$ replaced by the actual velocity of the follower $\boldsymbol{v}^n$. This results in the position error dynamics

$$\begin{aligned}\dot{\tilde{\boldsymbol{p}}}^n &= \boldsymbol{v}^n - \boldsymbol{v}_l^n = \boldsymbol{v}_d^n - \boldsymbol{v}_l^n + \tilde{\boldsymbol{v}}^n\\ &= \boldsymbol{v}_a^n + \tilde{\boldsymbol{v}}^n\end{aligned} \quad (18)$$

with $\tilde{\boldsymbol{v}}^n = \boldsymbol{v}^n - \boldsymbol{v}_d^n$ being the control error. Note that $\boldsymbol{v}_d^n = \boldsymbol{v}_a^n + \boldsymbol{v}_l^n$.

The error dynamics (18) together with tracking error dynamics, constitute the following error system that can be seen to have a cascaded systems structure:

$$\dot{\tilde{\boldsymbol{p}}}^n = \boldsymbol{v}_a^n + \tilde{\boldsymbol{v}}^n \quad (19a)$$

$$\dot{\boldsymbol{\xi}} = \Sigma\boldsymbol{\xi}. \quad (19b)$$

Theorem 1: The origin of the cascaded system (19) is UGAS.

Proof: The nominal dynamics of the cascade (19) consists of $\dot{\tilde{\boldsymbol{p}}}^n = \boldsymbol{v}_a^n$ and the velocity control error $\tilde{\boldsymbol{v}}^n$ is the perturbing term, which is trivially bounded. It is straightforward to show that the nominal dynamics are UGAS using the LFC (8) and it has already been shown that the perturbing dynamics are UGAS using the fact that Σ is Hurwitz. Consequently, the cascade (19) is UGAS according to [19, Lemma 2.1]. ■

Remark 8: Note that $\tilde{\boldsymbol{v}}^n$ is related to $\boldsymbol{\xi}$ through the transformation (13) and therefore forms the perturbing term of the nominal dynamics (19a).

Convergence of $\tilde{\boldsymbol{p}}^n$, u_r, ψ, and r to the desired values has thus been shown. However, in addition to the external dynamics given by (19), the system also has internal dynamics consisting of the underactuated sway dynamics. The stability properties of the complete system including both external and internal dynamics, remains to be analysed.

To analyse the underactuated sway dynamics, an additional cascade is formed using the sway dynamics (3e) and the closed loop system (19). Uniform global practical asymptotical stability (UGPAS) of the origin can then be shown using Theorem 8.26 from [20] (or [21, Theorem 1]), which is given in Appendix II.

Theorem 2: The cascaded system of internal and external dynamics given by

$$\dot{v}_r = X(u_r)r + Y(u_r)v_r \tag{20a}$$
$$\dot{\tilde{\boldsymbol{p}}}^n = \boldsymbol{v}_a^n + \tilde{\boldsymbol{v}}^n \tag{20b}$$
$$\dot{\boldsymbol{\xi}} = \Sigma\boldsymbol{\xi}. \tag{20c}$$

is uniformly globally practically asymptotically stable according to Theorem A.1.

Proof: Comparing (20) with (34) we have $x_1 = v_r$, $x_2 = [\tilde{\boldsymbol{p}}^n, \boldsymbol{\xi}]^T$, the parameter $\theta_1 = \dot{\psi}_{d,\max}$, and $\theta_2 = 0$. The perturbing dynamics $f_2(t, x_2)$ consist of (19) and by rewriting (20a) the nominal dynamics $f_1(t, x_1, \theta_1)$ and the perturbing dynamics $g(t, x, \theta)$ are given by

$$f_1(t, x_1, \theta_1) = Y(u_d)v_r + X(u_d)\dot{\psi}_d \tag{21}$$
$$\begin{aligned} g(t, x, \theta) = {} & X(\tilde{u}_r + u_d)\tilde{r} + \dot{\psi}_d\left(X(\tilde{u}_r + u_d) - X(u_d)\right) \\ & + v_r\left(Y(\tilde{u}_r + u_d) - Y(u_d)\right) \end{aligned} \tag{22}$$

In order to verify that Assumption A.1 holds, we analyse the perturbing term (22). It is easily verified that (22) is bounded in its arguments and that is vanishes when $\tilde{r}$ and $\tilde{u}_r$ are zero. Moreover, it should be noted that θ_2 is zero for this case. Therefore Assumption A.1 is satisfied.

Assumption A.2 requires the perturbing term dynamics to be UGPAS. As given by Theorem 1, the perturbing dynamics is UGAS, and Assumption A.2 is thus satisfied.

In order to verify that Assumption A.3 is satisfied, we use the following radially unbounded quadratic Lyapunov function candidate

$$V = \tfrac{1}{2}v_r^2 \tag{23}$$

with time derivative along the trajectories of v_r of the nominal dynamics

$$\begin{aligned} \dot{V} &= Y(u_d)v_r^2 + X(u_d)\dot{\psi}_d v_r \\ &\leq -Y_{\min}v_r^2 + X_{\max}\dot{\psi}_{d,\max}|v_r| \end{aligned} \tag{24}$$

which is negative definite for

$$|v_r| \geq \tfrac{X_{\max}}{Y_{\min}}\dot{\psi}_{d,\max}. \tag{25}$$

This assures Assumption A.3 is satisfied with

$$\delta_1 = \tfrac{X_{\max}}{Y_{\min}}\dot{\psi}_{d,\max}; \quad \theta_1 = \dot{\psi}_{d,\max} \tag{26}$$
$$\underline{\alpha}_{\delta_1}(|x_1|) = \tfrac{1}{2}v_r^2; \quad \overline{\alpha}_{\delta_1}(|x_1|) = 2v_r^2 \tag{27}$$
$$\alpha_{\delta_1} = Y_{\min}v_r^2 - \left|X_{\max}\dot{\psi}_{d,\max}v_r\right| \tag{28}$$
$$c_{\delta_1}(|x_1|) = 2|v_r|. \tag{29}$$

Consequently, UGPAS of the cascade (20) follows from Theorem A.1 and the proof of Theorem 2 is complete. ■

Remark 9: The results of the Lyapunov analysis show the trade-off that has to be made between how aggressively the leader is allowed to move (maximal yaw rate and speed) and the size of the ball $\mathcal{B}_{\delta_1}$ in which the induced sway velocity is not high enough to guarantee that (24) is negative definite.

Corollary 1: When the leader moves along a straight-line path the origin of the cascade (20) is UGAS.

TABLE I
SIMULATION PARAMETERS.

Variable	Value	Unit	Variable	Value	Unit
$U_{a,\max}$	5	m/s	k_ψ	0.04	-
$\Delta_{\tilde{p}}$	500	m	k_r	0.9	-
V_x	-1.1028	m/s	k_{u_r}	0.1	-
V_y	0.8854	m/s			

Proof: It is trivial to see that $\dot{\psi}_d$ will go to zero for a straight-line path and hence (24) becomes negative definite and the nominal dynamics are UGAS. Consequently, the origin of the cascade (20) is UGAS [19, Lemma 2.1]. ■

IV. SIMULATIONS

In this section two scenarios are used as case studies to validate the control strategy

1) the leader moves along a straight-line path that is at an angle with respect to the earth-fixed frame.
2) the leader moves along a sinusoidal path.

In both cases the follower ship is affected by a constant ocean current. The leader is represented by a point moving in the horizontal plane that is to be followed. This allows for a very straightforward implementation of the desired path and illustrates that the leader dynamics are not needed for the control strategy. Some parameters for the simulations are given in Table I. This includes the parameters for the controllers and guidance law, and the size of the ocean current. The follower vessel in the simulation is described by the ship model from [18].

A. Straight-line Path Following

The motion of the leader and the follower in the horizontal plane can be seen in Figure 2. From Figure 2 it can be seen that the follower converges to the trajectory of the leader and compensates for the current by side-slipping to maintain the desired path. The side-slipping is a desired result of the control strategy and is necessary to remain on the straight-line path in the presence of ocean currents. In particular, since the vessel is underactuated in sway a side-slip angle w.r.t. the path is necessary to compensate for the force pushing the vessel of the path. Since the desired heading angle is calculated from the inner- and outerproducts of the desired and actual velocity, the desired angle is the angle for which velocity error is zero, which is the necessary side-slip angle.

The synchronisation error in x and y can be seen in Figure 3. Figure 3 clearly shows that $\tilde{x}^n$ and $\tilde{y}^n$ converge to zero. Hence, target tracking or leader-follower synchronization with zero synchronisation error is attained.

B. Sinusoidal Path Following

The trajectory of the leader and the follower for tracking of a sinusoidal path can be seen in Figure 4. From Figure 4 it can be seen that the follower converges to the trajectory of the leader and compensates for the current to maintain the desired path.

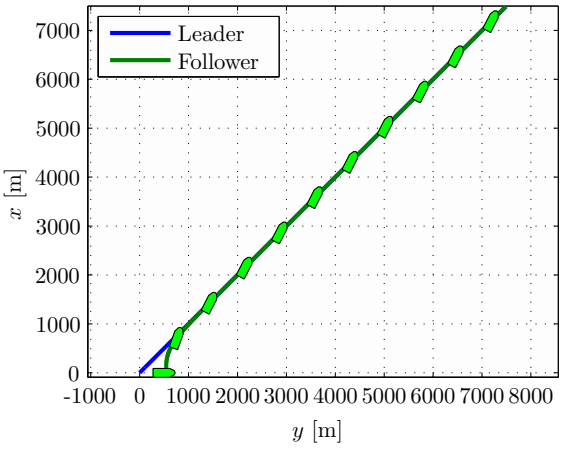

Fig. 2. Motion in the horizontal plane.

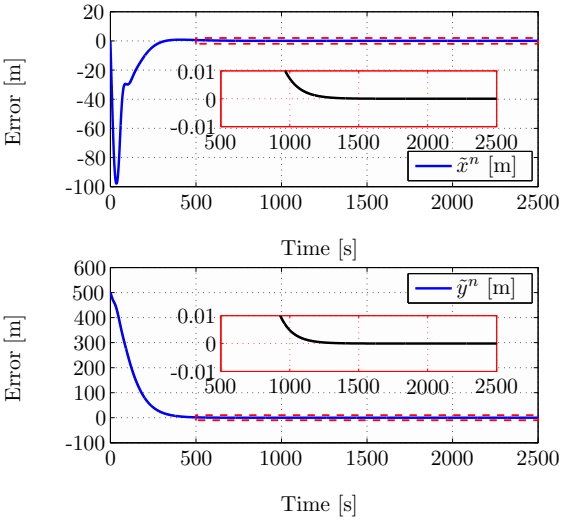

Fig. 3. x (top) and y (bottom) synchronisation error.

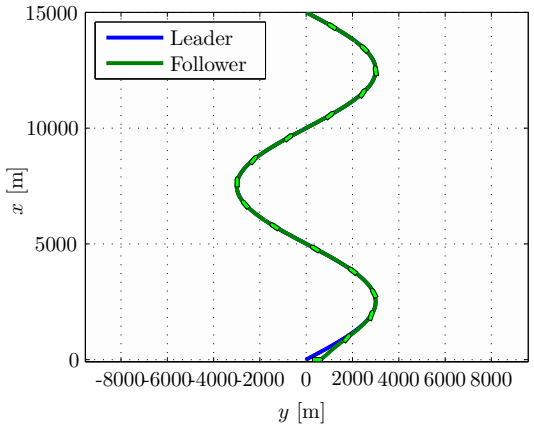

Fig. 4. Motion in the horizontal plane.

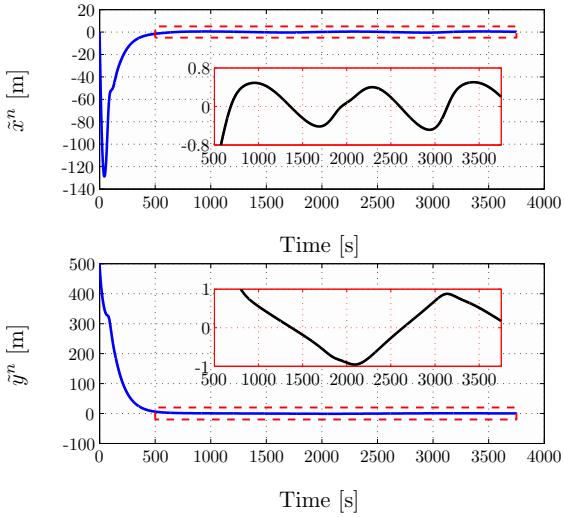

Fig. 5. x (top) and y (bottom) synchronisation error.

Figure 5 shows that the synchronisation error in both x and y do not fully converge to zero, but small oscillations persist. This corresponds with the stability analysis in Section III, which showed that a nonzero leader yaw rate will cause a perturbation in (20a) that cannot be suppressed by control action. In particular, the sway velocity component will cause a temporary misalignment of $\boldsymbol{v}^n$ and $\boldsymbol{v}_d^n$ that has to be corrected by the CB guidance algorithm. To relate these results to the stability proof we can plot the sway velocity v_r and $|X(u_d)|/|Y(u_d)|\dot{\psi}_d$ to evaluate (25). The results are shown in Figure 6 and from this figure it can be seen that v_r should make (24) negative definite and the conditions for the proof of UGPAS hold.

V. Conclusions

This paper has presented a control scheme for leader-follower synchronisation for inhomogeneous multi-agent systems consisting of an underactuated follower and a leader vessel with unknown dynamics. The developed leader-follower scheme can be applied to multi-agent systems with underactuated follower agents that are subjected to environmental disturbances. The dynamics of the leader is unknown, and the leader may be fully actuated or underactuated. Position and velocity measurements of the leader are available to the follower, while the trajectory of the leader is assumed to be unknown. The leader is free to move as it wants independently of the follower(s), and can for instance be manually controlled. The follower thus has no information about the future motion of the leader. The follower uses a constant bearing guidance algorithm to track the leader. Uniform global asymptotic stability of the origin of the error dynamics has been shown for straight-line paths, and uniform global practical asymptotic stability of the origin of the error dynamics has been shown for non-straight-line paths by analysing the closed-loop system together with the unactuated internal dynamics as a nonlinear cascaded system. The validity of the control scheme has been shown in a case study.

Appendix I
Function Definitions

The functions F_{u_r}, $X(u_r)$, $Y(u_r)$, and F_r are given by:

$$F_{u_r} \triangleq \frac{1}{m_{11}}(m_{22}v_r + m_{23}r)r - \frac{d_{11}}{m_{11}}u_r, \tag{30}$$

$$X(u_r) \triangleq \frac{m_{23}^2 - m_{11}m_{33}}{m_{22}m_{33} - m_{23}^2}u_r + \frac{d_{33}m_{23} - d_{23}m_{33}}{m_{22}m_{33} - m_{23}^2}, \tag{31}$$

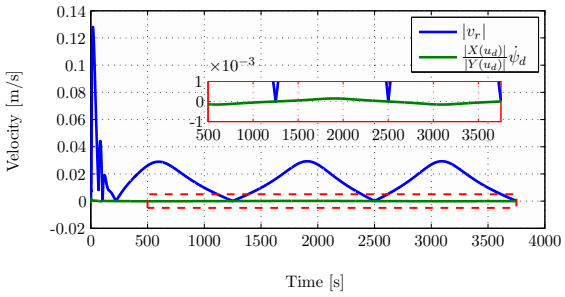

Fig. 6. Lyapunov bound on sway velocity.

$$Y(u_r) \triangleq \frac{(m_{22}-m_{11})m_{23}}{m_{22}m_{33}-m_{23}^2}u_r - \frac{d_{22}m_{33}-d_{32}m_{23}}{m_{22}m_{33}-m_{23}^2}, \tag{32}$$

$$F_r(u_r,v_r,r) \triangleq \frac{m_{23}d_{22}-m_{22}(d_{32}+(m_{22}-m_{11})u_r)}{m_{22}m_{33}-m_{23}^2}v_r + \frac{m_{23}(d_{23}+m_{11}u_r)-m_{22}(d_{33}+m_{23}u_r)}{m_{22}m_{33}-m_{23}^2}r. \tag{33}$$

APPENDIX II
UNIFORM GLOBAL PRACTICAL ASYMPTOTICAL STABILITY OF CASCADED SYSTEMS

This appendix presents Theorem 8.26 from [20] which considers UGPAS of cascaded systems. The theorem is used in the stability proof in Section III.

Theorem A.1: Under Assumptions A.1, A.2, and A.3, the cascaded system

$$\dot{x}_1 = f_1(t,x_1,\theta_1) + g(t,x,\theta) \tag{34}$$

$$\dot{x}_2 = f_2(t,x_2,\theta_2) \tag{35}$$

is uniformly globally practically asymptotically stable on the parameter set $\Theta_1 \times \Theta_2$.

Assumption A.1: The function g is uniformly bounded both in time and in θ_2 and vanishes with x_2, i.e., for any $\theta_1 \in \Theta_1$, there exists a nondecreasing function G_{θ_1} and a class $\mathcal{K}$ function Ψ_{θ_1} such that, for all $\theta_2 \in \Theta_2$, all $x \in \mathbb{R}^{n_1} \times \mathbb{R}^{n_2}$ and all $t \in \mathbb{R}_{\geq 0}$,

$$|g(t,x,\theta)| \leq G_{\theta_1}(|x|)\Psi_{\theta_1}(|x_2|) \tag{36}$$

Assumption A.2: The perturbing dynamics are UGPAS.

Assumption A.3: Given any $\delta_1 > 0$, there exist a parameter $\theta_1^\star(\delta_1) \in \Theta_1$, a continuously differentiable Lyapunov function V_{δ_1}, class $\mathcal{K}_\infty$ functions $\underline{\alpha}_{\delta_1}$, $\overline{\alpha}_{\delta_1}$, α_{δ_1} and a continuous positive nondecreasing function c_{δ_1} such that, for all $x_1 \in \mathbb{R}^n \backslash \mathcal{B}_{\delta_1}$ and all $t \in \mathbb{R}_{\geq 0}$,

$$\underline{\alpha}_{\delta_1}(|x_1|) \leq V_{\delta_1}(t,x_1) \leq \overline{\alpha}_{\delta_1}(|x_1|) \tag{37}$$

$$\frac{\partial V_{\delta_1}}{\partial t}(t,x_1) + \frac{\partial V_{\delta_1}}{\partial x_1}(t,x_1)f_1(t,x_1,\theta_1^\star) \leq -\alpha_{\delta_1}(|x_1|) \tag{38}$$

$$\left|\frac{\partial V_{\delta_1}}{\partial x}(t,x_1)\right| \leq c_{\delta_1}(|x_1|)) \tag{39}$$

$$\lim_{\delta_1 \to 0} \underline{\alpha}_{\delta_1}^{-1} \circ \overline{\alpha}_{\delta_1} = 0 \tag{40}$$

In addition, for the function G_{θ_1} of Assumption A.1, it holds that, for all $\delta_1 > 0$ and as s tends to $+\infty$,

$$c_{\delta_1}(s)G_{\theta_1^\star}(s) = \mathcal{O}(\alpha_{\delta_1}(s) \circ \overline{\alpha}_{\delta_1}^{-1}(s) \circ \underline{\alpha}_{\delta_1}(s)) \tag{41}$$

$$\alpha_{\delta_1} = \mathcal{O}(\overline{\alpha}_{\delta_1}(s)) \tag{42}$$

Definition 1: Following [21] given $a \in [-\infty;+\infty]$ and two functions $f_1, f_2 : \mathbb{R} \to \mathbb{R}$, we say that $f_1(s) = \mathcal{O}(f_2(s))$ as $s \to a$ if there exists a nonnegative constant b such that $|f_1(s)| < b|f_2(s)|$ in a neighbourhood of a.

REFERENCES

[1] E. Kyrkjebø, K. Y. Pettersen, M. Wondergem, and H. Nijmeijer, "Output synchronization control of ship replenishment operations: Theory and experiments," *Control Engineering Practice*, vol. 15, no. 6, pp. 741–755, 2007.

[2] R. Skejic, M. Breivik, T. I. Fossen, and O. M. Faltinsen, "Modeling and control of underway replenishment operations in calm water," in *8th Manoeuvring and Control of Marine Craft, Guarujá, Brazil*, 2009, pp. 78–85.

[3] H. Nijmeijer and A. Rodriguez-Angeles, *Synchronization of mechanical systems*. World Scientific, 2003.

[4] M. Breivik and T. I. Fossen, "Guidance laws for planar motion control," in *Proc. of the 47th IEEE Conference on Decision and Control, Cancun, Mexico*, 2008, pp. 570–577.

[5] S. H. Fu and W. M. Haddad, "Nonlinear adaptive tracking of surface vessels with exogenous disturbances," *Asian Journal of Control*, vol. 5, no. 1, pp. 88–103, 2003.

[6] A. A. Aguirre, "Remote control and motion coordination of mobile robots," Ph.D. dissertation, Technische Universiteit Eindhoven, 2011.

[7] J. P. Desai, J. P. Ostrowski, and V. Kumar, "Modeling and control of formations of nonholonomic mobile robots," *IEEE Transactions on Robotics and Automation*, vol. 17, no. 6, pp. 905–908, 2001.

[8] H. A. Poonawala, A. C. Satici, and M. W. Spong, "Leader-follower formation control of nonholonomic wheeled mobile robots using only position measurements, istanbul, turkey," in *9th Asian Control Conference (ASCC)*, June 2013, pp. 1–6.

[9] J. Dasdemir and A. Loria, "Robust formation-tracking control of mobile robots via one-to-one time-varying communication," *International Journal of Control*, pp. 1–17, 2014.

[10] M. Breivik, V. E. Hovstein, and T. I. Fossen, "Ship formation control: A guided leader-follower approach," in *Proc. IFAC World Congress, Seoul, Korea*, 2008.

[11] W. Caharija, K. Y. Pettersen, and J. T. Gravdahl, "Path following of marine surface vessels with saturated transverse actuators," in *American Control Conference (ACC), Washington, USA*, 2013, pp. 546–553.

[12] W. M. Haddad, S. G. Nersesov, Q. Hui, and M. Ghasemi, "Flocking and rendezvous control protocols for nonlinear dynamical systems via hybrid stabilization of sets," in *IEEE Proc. 52nd Conference on Decision and Control (CDC), 2013*. IEEE, 2013, pp. 2151–2156.

[13] Z. Peng, D. Wang, Z. Chen, X. Hu, and W. Lan, "Adaptive dynamic surface control for formations of autonomous surface vehicles with uncertain dynamics," *IEEE Transactions on Control Systems Technology*, vol. 21, no. 2, pp. 513–520, 2013.

[14] D. J. W. Belleter and K. Y. Pettersen, "Path following for formations of underactuated marine vessels under influence of constant ocean currents," in *Proceedings of the 53th IEEE Conference on Decision and Control, Los Angeles, USA, Dec. 15-17*, 2014, pp. 4521–4528.

[15] M. Breivik, V. E. Hovstein, and T. I. Fossen, "Straight-line target tracking for unmanned surface vehicles," *Modeling Identification and Control*, vol. 29, no. 4, pp. 131–149, 2008.

[16] E. Kyrkjebø, "Motion coordination of mechanical systems," Ph.D. dissertation, Norwegian University of Science and Technology, 2007.

[17] T. I. Fossen, *Handbook of Marine Craft Hydrodynamics and Motion Control*. Wiley, 2011.

[18] E. Fredriksen and K. Y. Pettersen, "Global κ-exponential way-point maneuvering of ships: Theory and experiments," *Automatica*, vol. 42, no. 4, pp. 677–687, 2006.

[19] A. Loría and E. Panteley, "Cascaded nonlinear time-varying systems: Analysis and design," in *Advanced topics in control systems theory*. Springer, 2005, pp. 23–64.

[20] A. Chaillet, "On stability and robustness of nonlinear systems," Ph.D. dissertation, Université Paris XI Orsay, 2006.

[21] A. Chaillet and A. Loría, "Uniform global practical asymptotic stability for time-varying cascaded systems," *European journal of control*, vol. 12, no. 6, pp. 595–605, 2006.